

# Stochastic Algorithms for Large-Scale Composite Optimization: the Case of Single-Shot X-FEL Imaging

D. Russell Luke\*

Steffen Schultze†

Helmut Grubmüller‡

January 25, 2024

## Abstract

We apply a recently developed framework for analyzing the convergence of stochastic algorithms to the general problem of large-scale nonconvex composite optimization more generally, and nonconvex likelihood maximization in particular. Our theory is demonstrated on a stochastic gradient descent algorithm for determining the electron density of a molecule from random samples of its scattering amplitude. Numerical results on an idealized synthetic example provide a proof of concept. This opens the door to a broad range of algorithmic possibilities and provides a basis for evaluating and comparing different strategies. While this case study is very specific, it shares a structure that transfers easily to many problems of current interest, particularly in machine learning.

**2010 Mathematics Subject Classification:** Primary 65C40, 90C06, 90C26; Secondary 46N30, 60J05, 49M27, 65K05.

**Keywords:** Nonconvex optimization, Large-scale optimization, Markov chain, Random function iteration, Error bounds, Convergence rates, Machine learning, Reinforcement learning, X-FEL imaging

## 1 Introduction

We study randomized algorithms for large-scale composite optimization models of the form

$$\min_{x \in \mathbb{R}^n} \sum_{j=0}^M g_j(x). \quad (\mathcal{P})$$

This problem format is the starting point for most applications in machine learning, but our particular interest in this model comes from electronic structure determination in X-ray imaging. The majority of the functions  $g_j$  are assumed to be smooth and nonconvex, though hard constraints and other sharp features can be incorporated through reserving  $g_0$  and the lower registers for nonsmooth functions. The indicator function of a closed set  $A \subset \mathbb{R}^n$ , for instance, is defined by

$$g_0(x) = \begin{cases} 0 & \text{if } x \in A \\ +\infty & \text{else.} \end{cases}$$

---

This research was funded by the Deutsche Forschungsgemeinschaft (DFG, German Research Foundation) – Project-ID 432680300 – SFB 1456, Project C02. DRL would like to thank Haven Sturm Luke for making his gaming computer available for this research.

\*Institut für Numerische und Angewandte Mathematik, Universität Göttingen, Lotzestr. 16–18, 37083 Göttingen, Germany. E-mail: [r.luke@math.uni-goettingen.de](mailto:r.luke@math.uni-goettingen.de).

†Max Planck Institute for Multidisciplinary Sciences, Department of Theoretical and Computational Biophysics, 37077, Göttingen. [steffen.schultze@mpinat.mpg.de](mailto:steffen.schultze@mpinat.mpg.de).

‡Max Planck Institute for Multidisciplinary Sciences, Department of Theoretical and Computational Biophysics, 37077, Göttingen. [hgrubmu@mpinat.mpg.de](mailto:hgrubmu@mpinat.mpg.de).

In the literature for this simple problem format, two main *computational* challenges are addressed: (a)  $n$  is large, and (b)  $M$  is large. We will focus on the latter challenge, though the analytical framework we apply is not limited to this situation alone. Of course issues like nonsmoothness and nonconvexity of the functions  $g_j$  are important considerations, but these are more consequential for the analysis than the implementation. The challenge of having too many variables is mainly handled by *coordinate descent* methods. For a demonstration of the application of our framework to stochastic coordinate descent see [21]. The main computational challenge for the application we have in mind is that the number of functions in the sum is enormous, which these days means  $M \approx 10^9$ . The standard numerical approach to handling this situation is to apply an iterative scheme using only a subset of the functions  $g_j$  at each iteration; randomized algorithms select a subset at random.

In a series of papers [14–16] Luke and collaborators developed a general convergence theory for randomized algorithms. The approach views such algorithms as Markov chains and convergence is in the sense of distribution with respect to the Prokhorov-Lévy (weak) or Wasserstein (strong) metrics in the space of probability distributions, depending on the assumptions. Verifying the assumptions of the theory boils down to analyzing the properties of the randomly selected/generated operators at the heart of the randomized algorithm. The application of this theory to single-shot X-FEL imaging was briefly described in [16]. In this context, we present here a deep-dive into a randomized method for computing the maximum likelihood estimator. We demonstrate the approach on simulated data for single-shot X-FEL imaging. While this case study is very specific, it shares a structure that transfers easily to many problems of current interest, particularly in machine learning. Beyond demonstrating the application of recent theory, one of the main contributions of this work is to add a benchmark problem instance for testing randomized splitting algorithms.

For the specific application of single-shot X-FEL we present a gradient descent algorithm for minimizing the negative log-likelihood of a given set of outcomes conditioned on a parameterization of a given stochastic model. In section 4.1 we show how this is an instance of *random function iterations* studied in [14–16], and present numerical results in section 4.2. Since our general approach reaches far beyond the specific application, we begin in section 2 with a general presentation of random function iterations for composite optimization.

## 2 Randomized composite optimization, stochastic feasibility, and abstract convergence

The abstract algorithmic template is very simple. We consider the collection of subsets of  $\{0, 1, \dots, M\}$  with cardinality  $m < M$ ,  $\mathbb{I} := \{I \in 2^{\{0,1,\dots,M\}} \mid |I| = m\}$ , indexed by  $i = 1, 2, \dots, M_m := \binom{M}{m}$  and construct operators  $T_i : G \rightarrow G$  for  $G \subset \mathbb{R}^n$ , tailored to each of the subsets  $I_i \in \mathbb{I}$ . To avoid some challenging technicalities, we will assume that  $T_i$  is at least continuous on  $G$  for all  $i$ . For instance, in the simplest incarnation of  $(\mathcal{P})$ , all of the functions  $g_i$  are smooth and  $T_i$  could be the steepest descent operator of the partial sum,

$$T_i := \frac{1}{m} \sum_{j \in I_i} T'_j \quad \text{where} \quad T'_j := (\text{Id} - t_j \nabla_j g_j). \quad (1)$$

This is just one of many possibilities. The main thing to observe here is that the mapping  $T_i$  is built by a convex combination of the elements  $T'_j$ . The regularity of the mapping  $T_i$  is determined by the calculus of *almost  $\alpha$ -firmly nonexpansive ( $\alpha$ -fne) mappings* [25, Proposition 2.4]  $T'_j$  whose regularity, in turn, is determined by the regularity of the functions  $g_j$ . The abstract randomized algorithm takes the form of Algorithm 1. The notation  $\mathbb{N}$  in the statement of Algorithm 1 denotes the natural numbers including 0. The initialization of this algorithm is stochastic in that we choose a random variable  $X_0$  with distribution  $\mu_0 \in \mathcal{P}(\mathbb{R}^n)$  where  $\mathcal{P}(\mathbb{R}^n)$  is the space of probability measures on  $\mathbb{R}^n$ ; practically, however, most algorithms will be initialized with a single deterministic point  $x_0$ , that is, the initial distribution is a delta distribution  $\mu_0 = \delta_{x_0}$ . Convergence of the iterates  $X_{k+1}$  depends not only on the properties of the mappings  $T_i$  (quasi-contractivity, for instance) but also on *consistency* of the fixed points of the individual mappings  $T_i$ . A

---

**Algorithm 1:** Random Function Iteration (RFI)

---

**Initialization:** Select a random variable  $X_0$  with distribution  $\mu_0 \in \mathcal{P}(\mathbb{R}^n)$ , and  $(\xi_k)_{k \in \mathbb{N}}$  an i.i.d. sequence with values on  $\{1, 2, \dots, M_m\}$ , where  $X_0$  and  $(\xi_k)$  are independently distributed. Given  $T_i : \mathbb{R}^n \rightarrow \mathbb{R}^n$  for  $i = 1, 2, \dots, M_m$ .

**for**  $k = 0, 1, 2, \dots$  **do**

$$X_{k+1} = T_{\xi_k}(X_k) \tag{2}$$

---

necessary condition for *almost sure* convergence of the sequence of random variables  $(X_k)_{k \in \mathbb{N}}$  is that the mappings  $T_i$  have common fixed points, that is  $\bigcap_i \text{Fix } T_i \neq \emptyset$  [15, Proposition 2.5]. This is a very strong assumption that allows one to dispense with a stochastic analysis entirely, deriving convergence guarantees from the available deterministic theory [14].

In the absence of common fixed points, the conventional approach is to examine the arithmetic mean of the sequence  $\bar{X}_k := \frac{1}{k} \sum_j^k X_k$ . The sequence of arithmetic means is referred to as the *ergodic sequence* in the optimization literature, the limit of this sequence, when it exists, is the *Cesàro sum*. We take a more general approach that can quantify not only convergence to the Cesàro sum, but also convergence of higher moments of the law of the iterates. This is achieved by viewing Algorithm 1 as a *Markov chain* whose iterates converge *in distribution* to an *invariant measure* of the corresponding Markov operator  $\mathcal{P}$ .

## 2.1 Notation and Definitions

Our notation is standard. The measurable sets are given by the Borel sigma algebra on a subset  $G \subset \mathbb{R}^n$ , denoted by  $\mathcal{B}(G)$ . When the law of  $X$ , denoted  $\mathcal{L}(X)$ , satisfies  $\mathcal{L}(X) = \mu$ , we write  $X \sim \mu \in \mathcal{P}(G)$ . Where convenient, we will also use the notation  $\mathbb{P}(X \in \cdot)$  to denote the law of the random variable, where  $\mathbb{P}$  is the probability measure on some underlying probability space. The *support of the probability measure*  $\mu$  is the smallest closed set  $A$ , for which  $\mu(A) = 1$  and is denoted by  $\text{supp } \mu$ .

The distance of a point  $x \in \mathbb{R}^n$  to a set  $A \subset \mathbb{R}^n$  in the metric  $d$  is denoted by  $d(x, A) := \inf_{w \in A} d(x, w)$ . The *projector* onto a set  $A$  is denoted by  $P_A$  and  $P_A(x)$  is the set of all points where  $d(x, A)$  is attained. This is empty if  $A$  is open, and a singleton if  $A$  is closed and convex; generically,  $P_A$  is a (possibly empty) set-valued mapping, for which we use the notation  $P_A : \mathbb{R}^n \rightrightarrows \mathbb{R}^n$ .

The following assumptions hold throughout.

**Assumption 1.** (a)  $\xi$  and  $\xi_0, \xi_1, \dots, \xi_k$  are i.i.d random variables for all  $k \in \mathbb{N}$  on a probability space with values on  $\{1, 2, \dots, M_m\}$ . The variable  $X_0$  is a random variable with values on  $\mathbb{R}^n$ , independent from  $\xi_k$ .

(b) The function  $\Phi : \mathbb{R}^n \times \{1, 2, \dots, M_m\} \rightarrow \mathbb{R}^n$ ,  $(x, i) \mapsto T_i x$  is measurable.

Let  $(X_k)_{k \in \mathbb{N}}$  be a sequence of random variables with values on  $G \subset \mathbb{R}^n$ . In [15] it is shown that the sequence of random variables  $(X_k)$  generated by Algorithm 1 is a Markov chain with transition kernel  $p$  given by

$$(x \in G)(A \in \mathcal{B}(G)) \quad p(x, A) := \mathbb{P}(T_\xi x \in A) \tag{3}$$

for the measurable *update function*  $\Phi : G \times \{1, 2, \dots, M_m\} \rightarrow G$  given by  $\Phi(x, i) := T_i x$ . Recall that a Markov chain with *transition kernel*  $p$  satisfies

(i)  $\mathbb{P}(X_{k+1} \in A \mid X_0, X_1, \dots, X_k) = \mathbb{P}(X_{k+1} \in A \mid X_k)$ ;

(ii)  $\mathbb{P}(X_{k+1} \in A \mid X_k) = p(X_k, A)$

for all  $k \in \mathbb{N}$  and  $A \in \mathcal{B}(G)$  almost surely in probability,  $\mathbb{P}$ -a.s. The Markov operator  $\mathcal{P}$  associated with this Markov chain is defined pointwise for a measurable function  $f : G \rightarrow \mathbb{R}$  via

$$(x \in G) \quad \mathcal{P}f(x) := \int_G f(y)p(x, dy),$$

when the integral exists. With the transition kernel defined above, we have

$$\mathcal{P}f(x) = \int_{\Omega} f(T_{\xi(\omega)}x) \mathbb{P}(d\omega).$$

The *dual* Markov operator acting on a measure  $\mu \in \mathcal{P}(G)$  is indicated by action on the right by  $\mathcal{P}$ :

$$(A \in \mathcal{B}(G)) \quad (\mathcal{P}^*\mu)(A) := (\mu\mathcal{P})(A) := \int_G \mathbb{P}(T_{\xi}x \in A) \mu(dx).$$

The distribution of the  $k$ 'th iterate of the Markov chain generated by Algorithm 1 is therefore easily represented as  $\mathcal{L}(X_k) = \mu_0\mathcal{P}^k$ .

An invariant measure of the Markov operator  $\mathcal{P}$  is any distribution  $\pi \in \mathcal{P}$  that satisfies  $\pi\mathcal{P} = \pi$ . The set of all invariant probability measures is denoted by  $\text{inv } \mathcal{P}$ . Of course in general random variables do not converge, but distributions associated with the sequence of random variables  $(X_k)$  of Algorithm 1, if they converge to anything, do so to invariant measures of the associated Markov operator. The stochastic algorithm (1) then solves the following *stochastic fixed point problem* [15, 16]:

$$\text{Find} \quad \pi \in \text{inv } \mathcal{P}. \quad (4)$$

When the mappings  $T_i$  have common fixed points (almost surely), the problem reduces to the *stochastic feasibility* problem studied in [8, 9, 14]:

$$\text{Find } x^* \in C := \{x \in G \mid \mathbb{P}(x = T_{\xi}x) = 1\}. \quad (5)$$

We use the *Wasserstein metric* for the space of measures to metrize convergence of the laws of the iterates of the Markov chain. Let

$$\mathcal{P}_2(G) = \left\{ \mu \in \mathcal{P}(G) \mid \exists x \in G : \int \|x - y\|^2 \mu(dy) < \infty \right\} \quad (6)$$

where  $\|\cdot\|$  is the Euclidean norm. The Wasserstein 2-metric on  $\mathcal{P}_2(G)$ , with respect to the Euclidean norm  $\|\cdot\|$  denoted  $d_{W_2}$ , is defined by

$$d_{W_2}(\mu, \nu) := \left( \inf_{\gamma \in \mathcal{C}(\mu, \nu)} \int_{G \times G} \|x - y\|^2 \gamma(dx, dy) \right)^{1/2} \quad (7)$$

where  $\mathcal{C}(\mu, \nu)$  is the set of couplings of  $\mu$  and  $\nu$ :

$$\mathcal{C}(\mu, \nu) := \{ \gamma \in \mathcal{P}(G \times G) \mid \gamma(A \times G) = \mu(A), \gamma(G \times A) = \nu(A) \quad \forall A \in \mathcal{B}(G) \}. \quad (8)$$

Since we are considering the Wasserstein 2-metric, convergence in this metric implies that also the second moments converge in this metric. For more background on the analysis of sequences of measures we refer interested readers to [4, 13, 37–39].

The Markov operator  $\mathcal{P}$  is *Feller* if  $\mathcal{P}f \in C_b(G)$  whenever  $f \in C_b(G)$ , where  $C_b(G)$  is the set of bounded and continuous functions from  $G$  to  $\mathbb{R}$ . Although this property is central to the theory of existence of invariant measures, we will assume existence of invariant measures. For us, the Feller property comes into play in characterizing the stationary points of Algorithm 1. It is a short exercise to show that if  $T_i$  is continuous for all  $i \in \{1, 2, \dots, M_m\}$  then the Markov operator  $\mathcal{P}$  is Feller (see [12, Theorem 4.22]). An elementary fact from the theory of Markov chains is that, if the Markov operator  $\mathcal{P}$  is Feller and  $\pi$  is a cluster point of the sequence of measures  $(\mu_k) := (\mu_0\mathcal{P}^k)$  with respect to convergence in distribution then  $\pi$  is an invariant probability measure [13, Theorem 1.10]. Moreover, the set of invariant measures of a Feller Markov operator is closed with respect to the topology of convergence in distribution [12, Section 5]. For more on this theory readers are referred to the cited works of Hairer and also [4].

## 2.2 Abstract Quantitative Convergence

We can now state the main theorem concerning Markov operators  $\mathcal{P}$  with transition kernel  $p$  given by (3) for self mappings  $T_i : G \rightarrow G$ . For any  $\mu_0 \in \mathcal{P}_2(G)$ , we denote the distributions of the iterates of Algorithm 1 by  $\mu_k = \mu_0 \mathcal{P}^k = \mathcal{L}(X_k)$ . It will be assumed that  $\text{inv } \mathcal{P} \neq \emptyset$ .

Convergence is quantified by an implicitly defined gauge function. Recall that  $\mathcal{G} : [0, \infty) \rightarrow [0, \infty)$  is a *gauge function* if  $\mathcal{G}$  is continuous, strictly increasing with  $\mathcal{G}(0) = 0$ , and  $\lim_{t \rightarrow \infty} \mathcal{G}(t) = \infty$ . The gauge  $\mathcal{G}$  is constructed implicitly from another nonnegative function  $\theta_{\tau, \epsilon} : [0, \infty) \rightarrow [0, \infty)$  with parameters  $\tau > 0$  and  $\epsilon \geq 0$  satisfying

$$(i) \theta_{\tau, \epsilon}(0) = 0; \quad (ii) 0 < \theta_{\tau, \epsilon}(t) < t \quad \forall t \in (0, \bar{t}] \text{ for some } \bar{t} > 0 \quad (9)$$

and

$$\mathcal{G} \left( \left( \frac{(1 + \epsilon)t^2 - (\theta_{\tau, \epsilon}(t))^2}{\tau} \right)^{1/2} \right) = t \quad \iff \quad \theta_{\tau, \epsilon}(t) = \left( (1 + \epsilon)t^2 - \tau (\mathcal{G}^{-1}(t))^2 \right)^{1/2} \quad (10)$$

for  $\tau > 0$  fixed. In the next theorem the parameter  $\epsilon$  quantifies the regularity of the generating mappings  $T_i$ ; the parameter  $\tau$  is directly computed from the another constant  $\alpha$  used to characterize the regularity of  $T_i$ .

In preparation for the results that follow, we will require at least one of the additional assumptions on  $\theta_{\tau, \epsilon}$ .

**Assumption 2.** *At least one of the following holds.*

(a)  $\theta_{\tau, \epsilon}$  satisfies

$$\theta_{\tau, \epsilon}^{(k)}(t) \rightarrow 0 \text{ as } k \rightarrow \infty \quad \forall t \in (0, \bar{t}), \quad (11)$$

and the sequence  $(\mu_k)$  is Fejér monotone with respect to  $\text{inv } \mathcal{P} \cap \mathcal{P}_2(G)$ , i.e.

$$d_{W_{2, \mathbf{p}}}(\mu_{k+1}, \pi) \leq d_{W_{2, \mathbf{p}}}(\mu_k, \pi) \quad \forall k \in \mathbb{N}, \forall \pi \in \text{inv } \mathcal{P} \cap \mathcal{P}_2(G); \quad (12)$$

(b)  $\theta_{\tau, \epsilon}$  satisfies

$$\sum_{j=1}^{\infty} \theta_{\tau, \epsilon}^{(j)}(t) < \infty \quad \forall t \in (0, \bar{t}) \quad (13)$$

where  $\theta_{\tau, \epsilon}^{(j)}$  denotes the  $j$ -times composition of  $\theta_{\tau, \epsilon}$ .

When  $\mathcal{G}$  is simply a linear gauge this becomes

$$\mathcal{G}(t) = \kappa t \quad \iff \quad \theta_{\tau, \epsilon}(t) = \left( (1 + \epsilon) - \frac{\tau}{\kappa^2} \right)^{1/2} t \quad (\kappa \geq \sqrt{\frac{\tau}{1 + \epsilon}}).$$

The conditions in (9) in this case simplify to  $\theta_{\tau, \epsilon}(t) = \gamma t$  where

$$0 < \gamma := 1 + \epsilon - \frac{\tau}{\kappa^2} < 1 \quad \iff \quad \sqrt{\frac{\tau}{1 + \epsilon}} \leq \kappa \leq \sqrt{\frac{\tau}{\epsilon}}. \quad (14)$$

In other words,  $\theta_{\tau, \epsilon}(t) = \gamma t$  for  $\gamma < 1$  satisfies Assumption 2(b). The weaker Assumption 2(a) is used to characterize sublinear convergence.

**Proposition 1** (convergence rates, Theorem 2.6, [16]). *Let  $G \subset \mathbb{R}^n$  be compact, let  $T_i : G \rightarrow G$  be continuous for all  $i \in \{1, 2, \dots, M_m\}$ , and let  $\xi$  and  $\xi_k$  ( $k \in \mathbb{N}$ ) be i.i.d. random variables taking values on  $\{1, 2, \dots, M_m\}$ . Define the Markov transport discrepancy  $\Psi : \mathcal{P}_2(G) \rightarrow \mathbb{R}_+ \cup \{+\infty\}$  by*

$$\Psi(\mu) := \inf_{\pi \in \text{inv } \mathcal{P}} \inf_{\gamma \in C_*(\mu, \pi)} \left( \int_{G \times G} \mathbb{E} \left[ \|(x - T_{\xi} x) - (y - T_{\xi} y)\|^2 \right] \gamma(dx, dy) \right)^{1/2}. \quad (15)$$

Assume furthermore:

(a) There is at least one  $\pi \in \text{inv } \mathcal{P} \cap \mathcal{P}_2(G)$  where  $\mathcal{P}$  is the Markov operator generated by  $T_i x$  (see (3));

(b)  $T_i$  satisfies

$$\begin{aligned} \exists \epsilon \in [0, 1), \alpha \in (0, 1) : \quad & \forall x \in G, \forall y \in \bigcup_{\pi \in \text{inv } \mathcal{P}} \text{supp}(\pi) \\ & \mathbb{E} \left[ \|T_\xi x - T_\xi y\|^2 \right] \leq (1 + \epsilon) d^2(x, y) - \frac{1-\alpha}{\alpha} \mathbb{E} \left[ \|(x - T_\xi x) - (y - T_\xi y)\|^2 \right]; \end{aligned} \quad (16)$$

(c)  $\Psi(\pi) = 0 \iff \pi \in \text{inv } \mathcal{P}$ , and for all  $\mu \in \mathcal{P}_2(G)$

$$d_{W_2}(\mu, \text{inv } \mathcal{P}) \leq \mathcal{G}(d_{\mathbb{R}}(0, \Psi(\mu))) = \mathcal{G}(\Psi(\mu)) \quad (17)$$

with gauge  $\mathcal{G}$  given implicitly by (10) with  $\tau = (1 - \alpha)/\alpha$  and the function  $\theta_{\tau, \epsilon}$  satisfying (9) where  $t_0 := d_{W_2}(\mu_0, \text{inv } \mathcal{P} \cap \mathcal{P}_2(G)) < \bar{t}$  for all  $\mu_0 \in \mathcal{P}_2(G)$ .

Then for any  $\mu_0 \in \mathcal{P}_2(G)$  the distributions  $(\mu_k)$  of the iterates of Algorithm 1 satisfy

$$d_{W_2}(\mu_{k+1}, \text{inv } \mathcal{P}) \leq \theta_{\tau, \epsilon}(d_{W_2}(\mu_k, \text{inv } \mathcal{P})) \quad \forall k \in \mathbb{N}. \quad (18)$$

If in addition  $\theta_{\tau, \epsilon}$  satisfies either one of the conditions in Assumption 2, then  $\mu_k \rightarrow \pi^{\mu_0} \in \text{inv } \mathcal{P} \cap \mathcal{P}_2(G)$  as  $k \rightarrow \infty$  in the  $W_2$  metric with rate  $O(\theta_{\tau, \epsilon}(k))$  in the case of Assumption 2(a) and in the case of Assumption 2(b) with rate  $O(s_k(t_0))$  where  $s_k(t_0) := \lim_{N \rightarrow \infty} \sum_{j=k}^N \theta_{\tau, \epsilon}^{(j)}(t_0)$ .

Condition (16) is a slight relaxation of the condition given in Theorem 2.6 of [16] (they have the inequality holding for all  $y \in G$ , not just  $y$  on the supports of the invariant measures) but their proof also holds for this more general statement. Both assumptions (c) and (a) of Proposition 1 have deep roots in fixed point theory and variational analysis. The context is explained in more detail in the next section.

Recall that a sequence  $(\mu_k)$  on the metric space  $(\mathcal{P}_2(G), d_{W_2})$  is said to *converge R-linearly* to  $\pi$  with rate  $c \in [0, 1)$  when there exists a  $\beta > 0$  such that  $d_{W_2}(\mu_k, \pi) \leq \beta c^k \quad \forall k \in \mathbb{N}$ . The sequence  $(\mu_k)$  is said to *converge Q-linearly* to  $\pi$  with rate  $c \in [0, 1)$  if there is a constant  $c \in [0, 1)$  such that  $d_{W_2}(\mu_{k+1}, \pi) \leq c d_{W_2}(\mu_k, \pi) \quad \forall k \in \mathbb{N}$ . Q-linear convergence is encountered with contractive fixed point mappings, and this leads to a priori and a posteriori error estimates on the sequence [28, Chapter 9].

**Corollary 2** (Corollary 2.7, [16]). *Under the same assumptions as in Proposition 1, if  $\Psi$  satisfies (c) with gauge  $\mathcal{G}(t) = r \cdot t$  and constant  $r$  satisfying  $\sqrt{\frac{1-\alpha}{\alpha(1+\epsilon)}} \leq r < \sqrt{\frac{1-\alpha}{\alpha\epsilon}}$ , then the sequence of iterates  $(\mu_k)$  converges R-linearly to some  $\pi^{\mu_0} \in \text{inv } \mathcal{P} \cap \mathcal{P}_2(G)$ :*

$$d_{W_2}(\mu_{k+1}, \text{inv } \mathcal{P}) \leq c d_{W_2}(\mu_k, \text{inv } \mathcal{P}) \quad (19)$$

where  $c := \sqrt{1 + \epsilon - \left(\frac{1-\alpha}{r^2\alpha}\right)} < 1$  and  $r \geq r'$  satisfies  $r \geq \sqrt{(1-\alpha)/\alpha(1+\epsilon)}$ . If  $\text{inv } \mathcal{P}$  consists of a single point then convergence is Q-linear.

It is important to emphasize that R-linear convergence permits neither a priori nor a posteriori error estimates.

In the remainder of this study we determine the classes of functions  $g_j$  in  $(\mathcal{P})$  that satisfy the assumptions of Proposition 1 for a number of possible candidates for the mappings  $T_i$ . The concrete application of negative log-likelihood minimization in the context of X-FEL imaging falls into the identified function classes.

### 3 Regularity

Our main results concern convergence of Markov chains under regularity assumptions that are lifted from the generating mappings  $T_i$ . In [25] a framework was developed for a quantitative convergence analysis of set-valued mappings  $T_i$  that are one-sided Lipschitz continuous in the sense of set-valued-mappings with Lipschitz constant slightly greater than 1. We begin with the regularity of  $T_i$  and follow this through to the regularity of the resulting Markov operator.

### 3.1 Almost $\alpha$ -firmly nonexpansive mappings

Let  $G \subset \mathbb{R}^n$  and let  $F : G \rightarrow \mathbb{R}^n$ . The mapping  $F$  is said to be *pointwise almost  $\alpha$ -firmly nonexpansive at  $x_0 \in G$  on  $G$* , abbreviated *pointwise  $\alpha\alpha$ -fne* whenever

$$\begin{aligned} &\exists \epsilon \in [0, 1) \text{ and } \alpha \in (0, 1) : \\ &\|Fx - Fx_0\|^2 \leq (1 + \epsilon)\|x - x_0\|^2 - \frac{1-\alpha}{\alpha}\psi(x, x_0, Fx, Fx_0) \quad \forall x \in G, \end{aligned} \quad (20)$$

where the *transport discrepancy*  $\psi$  of  $F$  at  $x$  and  $x_0$  is defined by

$$\begin{aligned} \psi(x, x_0, Fx, Fx_0) &:= \\ &\|Fx - x\|^2 + \|Fx_0 - x_0\|^2 + \|Fx - Fx_0\|^2 + \|x - x_0\|^2 - \|Fx - x_0\|^2 - \|x - Fx_0\|^2. \end{aligned} \quad (21)$$

When the above inequality holds for all  $x_0 \in G$  then  $F$  is said to be  *$\alpha\alpha$ -fne on  $G$* . The *violation* is the constant  $\epsilon$  for which (20) holds. When  $\epsilon = 0$  the mapping  $F$  is said to be *(pointwise)  $\alpha$ -firmly nonexpansive*, abbreviated *(pointwise)  $\alpha$ -fne*.

The transport discrepancy  $\psi$  ties the regularity of the mapping to the geometry of the space. A short calculation shows that, in a Euclidean space, this has the representation

$$\psi(x, x_0, Fx, Fx_0) = \|(x - Fx) - (x_0 - Fx_0)\|^2. \quad (22)$$

The definition of pointwise  $\alpha\alpha$ -fne mappings in Euclidean spaces appeared first in [25] where they are called *pointwise almost averaged* mappings, following the historical development of these notions dating back to Mann, Krasnoselskii, and others [7, 11, 19, 26]. The terminology of “averaged mappings” comes from Baillon, Bruck and Reich [1]. We do not use this nomenclature because it does not accommodate nonlinear spaces where addition is not defined.

Condition (16) of Proposition 1 is the pointwise  $\alpha\alpha$ -fne property *in expectation* at points in the support of invariant measures. On a closed subset  $G \subset \mathbb{R}^n$  for a general self-mapping  $T_i : G \rightarrow G$  for  $i \in \{1, 2, \dots, M_m\}$ , the mapping  $\Phi : G \times \{1, 2, \dots, M_m\} \rightarrow G$  be given by  $\Phi(x, i) = T_i x$  is said to be *pointwise almost  $\alpha$ -firmly nonexpansive in expectation at  $x_0 \in G$  on  $G$* , abbreviated *pointwise  $\alpha\alpha$ -fne in expectation*, whenever

$$\begin{aligned} &\exists \epsilon \in [0, 1), \alpha \in (0, 1) : \quad \forall x \in G, \\ &\mathbb{E} [\|\Phi(x, \xi) - \Phi(x_0, \xi)\|^2] \leq (1 + \epsilon)\|x - x_0\|^2 - \frac{1-\alpha}{\alpha}\mathbb{E} [\psi(x, x_0, \Phi(x, \xi), \Phi(x_0, \xi))]. \end{aligned} \quad (23)$$

When the above inequality holds for all  $x_0 \in G$  then  $\Phi$  is said to be *almost  $\alpha$ -firmly nonexpansive ( $\alpha\alpha$ -fne) in expectation on  $G$* . The expected violation is a value of  $\epsilon$  for which (23) holds. When the violation is 0, the qualifier “almost” is dropped and the abbreviation  *$\alpha$ -fne in expectation* is used.

**Example 1** (steepest descent mappings of smooth functions are  $\alpha\alpha$ -fne). *Let  $g : \mathbb{R}^n \rightarrow \mathbb{R}$  be continuously differentiable with Lipschitz, hypomonotone gradient, that is  $g$  satisfies*

$$\exists L > 0 : \quad \|\nabla g(x) - \nabla g(y)\|^2 \leq L^2\|x - y\|^2 \quad \forall x, y \in \mathbb{R}^n, \quad (24a)$$

and

$$\exists \tau \geq 0 : \quad -\tau\|x - y\|^2 \leq \langle \nabla g(x) - \nabla g(y), x - y \rangle \quad \forall x, y \in \mathbb{R}^n. \quad (24b)$$

Then a specialization of [21, Proposition 13] to just a single block mapping establishes that the gradient descent mapping defined by  $T_{GD} := \text{Id} - t\nabla g$  is  $\alpha\alpha$ -fne on  $\mathbb{R}^n$  with violation at most

$$\epsilon_{GD} = \left\{ 2t\tau + \frac{t^2 L^2}{\alpha} \right\} < 1, \quad \text{with constant } \alpha \quad (25a)$$

whenever the steps  $t$  satisfy

$$t \in \left( 0, \frac{\alpha\sqrt{\tau^2 + L^2} - \alpha\tau}{L^2} \right). \quad (25b)$$

If  $g$  is convex then, with step size  $t < \frac{2\alpha}{L}$  for  $\alpha \in (0, 1)$ , the gradient descent mapping  $T_{GD}$  is  $\alpha$ -fne with constant  $\alpha$  (no violation).

Notice the interdependence of the step  $t$  on the constant  $\alpha$ : if one is willing to tolerate a larger  $\alpha$ , then a larger step  $t$  is possible; this is at the cost, however, of increasing the violation. Also, the closer  $\alpha$  is to 1, the more expansive the steepest descent operator is, as seen by (20). On the other hand, short steps mean slow progress.

Now, using the calculus of  $\alpha\alpha$ -fne mappings [25, Proposition 2.4] this yields immediately the regularity of the steepest descent mapping of the partial sum in (1). Indeed,  $T_{GD_i} := \frac{1}{m} \sum_{j \in I_i} \text{Id} - t_j \nabla g_j$  for  $I_i \in \mathbb{I} := \{I \in 2^{\{0,1,\dots,M\}} \mid |I| = m\}$  is  $\alpha\alpha$ -fne on  $\mathbb{R}^n$  with violation at most

$$\epsilon_{GD_i} = \frac{1}{m} \sum_{j \in I_i} \left\{ 2t_j \tau_j + \frac{t_j^2 L_j^2}{\bar{\alpha}_i} \right\} < 1, \quad \text{with constant } \bar{\alpha}_i := \max_{j \in I_i} \alpha_j \quad (26a)$$

whenever the steps  $t_j$  satisfy

$$t_j \in \left( 0, \frac{\bar{\alpha}_i \sqrt{\tau_j^2 + L_j^2} - \bar{\alpha}_i \tau_j}{L_j^2} \right). \quad (26b)$$

Here  $L_j$  and  $\tau_j$  are the respective Lipschitz and hypomonotonicity constants of the individual functions  $g_j$  defined in (24).

In practice, it can also be expensive to draw a new sample  $I_i \in \mathbb{I}$  because this involves moving data into and out of memory on a computer. We therefore extend the basic partial gradient descent approach above to allow the option of taking several steepest descent steps on each single sample  $I_i$ . Here we have

$$T_i := T_{GD_i}^q = \left( \frac{1}{m} \sum_{j \in I_i} \text{Id} - t_j \nabla g_j \right)^q \quad (27)$$

where  $q \geq 1$  is some fixed number of times the steepest descent operator  $T_{GD_i}$  is applied. Again using the calculus of  $\alpha\alpha$ -fne mappings [25, Proposition 2.4] yields the regularity estimate that  $T_i$  is  $\alpha\alpha$ -fne on  $\mathbb{R}^n$  with violation at most

$$\epsilon_i = (1 + \epsilon_{GD_i})^q - 1, \quad \text{with constant at most } \alpha_i := \frac{q}{q - 1 + 1/\bar{\alpha}_i} \quad (28)$$

whenever the steps  $t_j$  satisfy (26b).

**Example 2** (incorporating nonsmooth functions). We mentioned that the first functions in the sum ( $\mathcal{P}$ ) are reserved for constraints and other nonsmooth functions. Suppose, that these are at least lower semicontinuous (lsc) and prox-friendly, meaning that the resolvent of the subdifferential has a closed form. By subdifferential, denoted  $\partial g_j$ , we mean the collection of all general/limiting subgradients [33, Definition 8.3]. Then one would use the resolvents of the subdifferentials of these functions:  $T'_j = J_{\partial g_j, t_j} := (\text{Id} + t_j \partial g_j)^{-1}$ . For  $g_j$  convex this is  $\alpha$ -fne with  $\alpha = 1/2$  [27]. More generally, we will assume that  $g_j$  is subdifferentially regular (the limiting subdifferential is nonempty on  $\text{dom } g_j$ ) with subdifferentials satisfying

$$\begin{aligned} \exists \tau_j \geq 0 : \quad & \forall x, u, v \in G \subset \mathbb{R}^n, \forall z \in t_j \partial g_j(u; x), w \in t_j \partial g_j(v; x), \\ & -\frac{\tau_j}{2} \|(u+z) - (v+w)\|^2 \leq \langle z - w, u - v \rangle. \end{aligned} \quad (29)$$

Then by [25, Proposition 2.3] the resolvent  $J_{\partial g_j, t_j}$  is  $\alpha\alpha$ -fne with constant  $\alpha_j = 1/2$  and violation  $\tau_j$  on  $G$ .

The regularity characterized by (29) was introduced in [25] and was shown in [23] to be a generalization of hypomonotonicity [30, 31, 36]; in particular, weakly convex functions (functions that, upon addition by a quadratic, can be made convex) satisfy (29), but the converse does not hold.



There are a number of ways to combine steepest descent steps with resolvents; we focus on the following generalized forward-backward mapping. Let  $g_j : \mathbb{R}^n \rightarrow \mathbb{R} \cup \{+\infty\}$  be lsc, prox-friendly and satisfy (29) for  $j = 0, 1, 2, \dots, s$  and satisfy (24) for  $j = s + 1, \dots, M$ . Then

$$T_i := \left( \left( \prod_{j \in I_i, j \leq s} J_{\partial g_j, t_j} \right) \circ \left( \frac{1}{m} \sum_{j \in I_i, j > s} \text{Id} - t_j \nabla g_j \right)^q \right)^r \quad (30)$$

where  $q, r \geq 1$  allow for repeated application of the respective operators, and the product  $\prod_{j \in I_i, j \leq s} J_{\partial g_j, t_j} = 1$  when there are no indexes  $j \in I_i$  with  $j \leq s$ . Application of the calculus of  $\alpha$ -fne mappings establishes that  $T_i$  given by (30) is  $\alpha$ -fne on  $G$  with violation

$$\epsilon_i = \left( \left( \prod_{j \in I_i, j \leq s} (1 + \tau_j) \right) (1 + \epsilon_{GD_i})^q \right)^r - 1, \quad (31a)$$

and with constant at most

$$\hat{\alpha}_i := \frac{r}{r - 1 + 1/\tilde{\alpha}_i} \quad \text{where} \quad \tilde{\alpha}_i := \frac{|I_i \setminus \{j > s\}| + 1}{|I_i \setminus \{j > s\}| + \max\{1/2, \alpha_i\}} \quad (31b)$$

for  $\alpha_i$  given by (28) for the steps  $t_j$  with  $j > s$  satisfying (26b). Note that the steps  $t_j$  for the nonsmooth function are only implicitly involved here through the constant  $\tau_j$  in (29). Here too, the larger the step  $t_j$ , the larger the constant  $\tau_j$ , which leads to a greater violation in (31a).

### 3.2 Metric subregularity of the invariant Markov transport discrepancy

Recall the inverse mapping  $\Psi^{-1}(y) := \{\mu \mid \Psi(\mu) = y\}$ , which clearly can be set-valued. It is important to keep in mind that an invariant measure need not correspond to a fixed point of any individual mapping  $T_i$ , unless these have common fixed points. See [15, 16] instances of this. Condition (17) together with positivity of  $\Psi$ , that is  $\Psi$  takes the value 0 at  $\mu$  if and only if  $\mu \in \text{inv } \mathcal{P}$ , is the assumption that  $\Psi$  is *gauge metrically subregular for 0 relative to  $\mathcal{P}_2(G)$  on  $\mathcal{P}_2(G)$*  [17]:

$$d_{W_2}(\mu, \text{inv } \mathcal{P}) = d_{W_2}(\mu, \Psi^{-1}(0)) \leq \mathcal{G}(\Psi(\mu)) \quad \forall \mu \in \mathcal{P}_2(G). \quad (32)$$

The gauge of metric subregularity  $\mathcal{G}$  is constructed implicitly from  $\theta_{\tau, \epsilon} : [0, \infty) \rightarrow [0, \infty)$  with parameters  $\tau > 0$  and  $\epsilon \geq 0$  satisfying (9) and (10) for  $\tau > 0$  fixed. In Proposition 1 the parameter  $\epsilon$  is exactly the expected violation in the update mappings  $\Phi(x, i) = T_i(x)$  which, as in Example 1 and 2, are  $\alpha$ -fne (see (23) and (16)); the parameter  $\tau$  is directly computed from the expected constant  $\alpha$  via  $\tau = (1 - \alpha)/\alpha$ .

When the mappings  $T_i$  have at least one common fixed point, then the feasible set is nonempty:

$$C := \{x \in G \mid \mathbb{P}(x \in T_\xi x) = 1\} = \bigcap_{i \in \{1, 2, \dots, M_m\}} \text{Fix } T_i \cap G \neq \emptyset. \quad (33)$$

Moreover, the set of measures supported on the feasible set is also nonempty, that is

$$\mathcal{C} := \{\pi \in \text{inv } \mathcal{P} \mid \text{supp}(\pi) \subset C\} \neq \emptyset \quad (34)$$

since the delta distribution centered at a point  $x^* \in C$  is in  $\mathcal{C}$ . The stochastic fixed point problem in this case is a consistent stochastic feasibility problem. Here the Markov transport discrepancy  $\Psi$  defined by (15) simplifies considerably. Indeed, take any  $\pi \in \mathcal{C}$ . Then for  $y \in \text{supp } \pi$  we have  $y = T_\xi y$  (almost surely) and

(15) becomes

$$\begin{aligned}
\Psi(\mu) &:= \inf_{\pi \in \text{inv } \mathcal{P}} \inf_{\gamma \in \mathcal{C}_*(\mu, \pi)} \left( \int_{G \times G} \mathbb{E} \left[ \|(x - T_\xi x) - (y - T_\xi y)\|^2 \right] \gamma(dx, dy) \right)^{1/2} \\
&= \inf_{\gamma \in \mathcal{C}_*(\mu, \delta_y)} \left( \int_{G \times G} \mathbb{E} \left[ \|x - T_\xi x\|^2 \right] \gamma(dx, dy) \right)^{1/2} \\
&= \left( \int_G \mathbb{E} \left[ \|x - T_\xi x\|^2 \right] \mu(dx) \right)^{1/2}.
\end{aligned} \tag{35}$$

Clearly  $\mu \in \mathcal{C}$  implies that  $\Psi(\mu) = 0$ . Condition (17) then reduces to

$$d_{W_2}(\mu, \text{inv } \mathcal{P}) \leq \mathcal{G} \left( \left( \int_G \mathbb{E} \left[ \|x - T_\xi x\|^2 \right] \mu(dx) \right)^{1/2} \right). \tag{36}$$

Suppose now that  $\mu$  is such that  $d_{W_2}(\mu, \text{inv } \mathcal{P})$  is attained at some  $\pi \in \mathcal{C}$ . Then

$$d_{W_2}(\mu, \mathcal{C}) = d_{W_2}(\mu, \text{inv } \mathcal{P}) \leq \mathcal{G} \left( \left( \int_G \mathbb{E} \left[ \|x - T_\xi x\|^2 \right] \mu(dx) \right)^{1/2} \right). \tag{37}$$

Writing this pointwise (i.e., for  $\mu = \delta_x$ ) reduces (17) to a recognizable (nonlinear) error bound, albeit in expectation:

$$d(x, C) = \inf_{z \in C} \|x - z\| \leq \mathcal{G}(\mathbb{E}[\|x - T_\xi x\|]) \quad \forall x \in G. \tag{38}$$

## 4 Case Study: likelihood maximization and X-FEL imaging

We specialize the composite minimization model to minimizing the negative log-likelihood function:

$$\underset{x \in C_0}{\text{minimize}} \ E(x) := \sum_{j=1}^M -\log(f(y_j; \phi(x))). \tag{39}$$

Here  $\phi : \mathbb{R}^n \rightarrow \mathbb{R}^m$  is a nonlinear but smooth map modelling a proposed probability distribution parameterized by  $x \in \mathbb{R}^n$ ,  $C_0 \subset \mathbb{R}^n$  is an abstract constraint set,  $y_j \in \mathbb{R}^m$  ( $j = 1, 2, \dots, M$ ) is an outcome, and  $f(y_j; \phi(x))$  is the *likelihood* of observing the outcome  $y_j$  with the probability distribution  $\phi(x)$ ,

$$f(y_j; \phi(x)) := \mathbb{P}_{\phi(x)}(Y_j = y_j). \tag{40}$$

The constraint  $x \in C_0$  is formally handled by adding to the sum (39) the indicator function

$$g_0(x) := \iota_{C_0}(x); \tag{41}$$

the other functions in the objective ( $\mathcal{P}$ ) are apparently

$$g_j(x) := -\log(f(y_j; \phi(x))). \tag{42}$$

The random variable  $Y_j$  has some unknown true probability distribution. The outcome  $y_j$  is the result of a sample from the probability distribution. We do not presume to approximate the true probability distribution, although, obviously this is the whole point of problem (39). Instead, we focus on numerical methods for solving (39) when the collection of outcomes  $\{y_1, y_2, \dots, y_M\}$  is too large to be handled all at once. Interpretation of solutions to (39) as well as the limit of these solutions as  $M \rightarrow \infty$  is a topic for mathematical statistics.

As long as  $f(y_j; \phi(x))$  is sufficiently smooth as a function of  $x$  and the constraint set  $C_0$  is sufficiently regular (for instance, closed and convex), then the regularity assumption (16) of Proposition 1 holds by the discussion in Examples 1 and 2; hence the random function iteration Algorithm 1 is a reasonable candidate for mappings  $T_i$  given by (30). We will show this is indeed the case for the concrete application of X-FEL imaging.

## 4.1 Stochastic tomography and single-shot X-FEL imaging

The goal of single-shot X-FEL imaging is to determine the electron density of a molecule from experimental samples of its scattering probability distribution (i.e. diffraction pattern) [6, 10, 41]. A two-dimensional measurement device, partitioned into pixels, counts the occurrence of (coherently scattered) photons in a three-dimensional domain in the far field of a molecule that has been illuminated by a short X-FEL pulse. The molecule under observation is at a random and unobservable orientation relative to the measurement device. The illuminating pulse is only long enough to cause a few (between 3 and 100) scattering events from the interaction of the X-ray beam with the electrons of the molecule. The experiment is repeated about  $10^9$  times, each time with the molecule at a different random orientation.

Image reconstruction from single-shot X-FEL experiments is a stochastic tomography problem with a nonlinear model for the data. The stochastic aspect comes not from the randomness of the molecule orientations (although this makes the problem harder), but rather from the random samples of the scattered field that constitute the data. The tomographic aspect comes from the challenge of reconstructing a three-dimensional object from two-dimensional data. Computed tomography with random orientations is not new (see [2] and [3]). When the orientations are not known, or in the case of single-shot X-FEL imaging unobservable, some earlier successful approaches applied to Radon inversion (a linear imaging model) involved estimating the orientation first, and then inverting the imaging model [29] and [35].

The problem investigated in [34] differs from [2, 3, 29, 35] in three respects. First and foremost, the model for the data in X-FEL imaging is nonlinear and nonconvex: Fraunhofer diffraction models the field propagation (mathematically equivalent to Fourier transformation, and thus linear), however the measurements are only *samples* of the *intensities* of the (complex-valued) field [5] and [40]. This leads to the second, equally important distinction, namely that the model data is truly a low-count sample from an unknown distribution (i.e. field intensities), which prohibits directly applying the already known techniques for phase retrieval from coherent diffraction data, as is done in X-ray crystallography [32]. The third departure from previous approaches is that the step of estimating the unknown orientation is avoided by computing the likelihood of the observation at *all combinations of orientations*.

Considering only *coherently scattered photons*, the problem is to determine the true three-dimensional electron density  $\rho_*$  from a collection of two-dimensional images  $\{y_{s_1}, y_{s_2}, \dots, y_{s_M}\}$ , where each  $y_{s_j}$  is an outcome, or sample from a two-dimensional cross section of the true three-dimensional probability distribution in the far field  $\phi_*$  at orientation  $s_j \in SO(3)$ , denoted  $\phi_*^{s_j}$ . The continuous model for the probability distribution in the far field  $\phi_* : \mathbb{R}^3 \rightarrow \mathbb{R}_+$  is derived from the planar Fraunhofer scattering model [5]

$$\phi_*^s(k) := |[\mathcal{F}(\rho_* \circ R(s))](k)|^2, \quad k \in \mathcal{E}. \quad (43)$$

Here  $\rho_* : \mathbb{R}^3 \rightarrow \mathbb{R}_+$  is the electron density,  $R(s) : \mathbb{R}^3 \rightarrow \mathbb{R}^3$  is a rotation operator that rotates the domain  $\mathbb{R}^3$  by  $s \in SO(3)$ ,  $\mathcal{F} : \mathbb{C}^3 \rightarrow \mathbb{C}^2$  is the Fraunhofer transform modelling the propagation of the electromagnetic field to a two-dimensional surface in the far field, and, in a nod to the physicists, we denote by  $k \in \mathbb{R}^3|_{\mathcal{E}}$  a point on a two-dimensional surface  $\mathcal{E}$  (the Ewald sphere) in the far field. Up to scaling,  $\mathcal{F}$  is just the Fourier transform. The function  $\phi_*^s(k)$  is the *intensity* of the field over long time spans and yields the probability of observing a photon at position  $k$  when the electron density  $\rho_*$  is rotated by  $s \in SO(3)$  and illuminated by an X-ray.

We approximate the true electron density with a function  $\rho(\cdot; x)$  parameterized by  $x \in C_0 \subset \mathbb{R}^n$ . The parameters are chosen so as to maximize the likelihood that random variables  $Y_{s_j}$  drawn from the true distribution  $\phi_*$  match the observed outcomes  $y_{s_j}$ , or equivalently, the optimal parameters  $x^*$  minimize the negative log-likelihood functional (39) over some constraint set  $C_0$ . This yields the following discretized model for the intensity

$$\phi^s(k; x) := |[\mathcal{F}(\rho(\cdot; x) \circ R(s))](k)|^2, \quad k \in \mathbb{R}^2, x \in \mathbb{R}^n. \quad (44)$$

In coherent diffraction imaging, the observations are over long time frames and the illuminating field is assumed not to damage the object being observed (whether electron densities or cells is just a matter of scale) [32]. In this scenario one simply takes the observations  $\{y_{s_1}, y_{s_2}, \dots, y_{s_M}\}$  to be identical to the

probability  $\phi^s(k; x)$  (when the rotation  $s$  is known). If enough photons are counted in each image, then the problem reduces to the conventional optical phase retrieval problem for which successful numerical algorithms abound [22]. In a sense, this is the situation when each image  $y_{s_j}$  is the true scattering density at orientation  $s_j$ , in which case expectation maximization really does find a best approximation of a reasonable parameterization to the true probability distribution.

In X-FEL imaging, the illuminating pulse destroys the molecule under observation, and so the time is kept very short so that one can record scattering events (anywhere from 3 to 100) from the molecule before it disintegrates. The observations  $\{y_1, y_2, \dots, y_M\}$  are therefore simply counts of photons in a plane,  $y_j(k) \in \mathbb{N}$  for  $k \in \mathbb{R}^2$ . This is modeled as a *Poisson point process*:

$$f(y_j(k); \phi^s(k; x)) = \mathbb{P}_{\phi^s(k; x)}(Y_j^s(k) = y_j(k)) := \frac{\phi^s(k; x)^{y_j(k)} \exp(-\phi^s(k; x))}{y_j(k)!} \quad (45a)$$

where  $f(y_j(k); \phi^s(k; x))$  is the likelihood function in (39). We have removed the dependence of the observation  $y_j$  on the rotation  $s$  since this is unobservable. We will come to this in a moment. Before accounting for the rotation, note that a single observation  $y_j$  consists of all counts at locations  $k \in \mathbb{R}^2$ , so the likelihood of  $y_j$  with simultaneous counts at all locations, assuming independence, is

$$\begin{aligned} f(y_j; \phi^s(\cdot; x)) &= \prod_{k \in \text{supp}(y_j)} \frac{\phi^s(k; x)^{y_j(k)} \exp(-\phi^s(k; x))}{y_j(k)!} \\ &= \exp\left(-\sum_{k \in \text{supp}(y_j)} \phi^s(k; x)\right) \prod_{k \in \text{supp}(y_j)} \frac{\phi^s(k; x)^{y_j(k)}}{y_j(k)!}. \end{aligned} \quad (45b)$$

**Remark 3** (modelling detector arrays). *Our numerical simulation adds the discretization of the two-dimensional detector in the Fourier domain ( $k$ -space, for the physicists) into pixels to the model (45b). Within a single pixel the exact location of the photon cannot be determined. Mathematically, this is modelled by partitioning each observation  $\text{supp}(y_j)$  into a rectangular grid. To avoid clutter, we will not explicitly represent this discretization in our derivation, but we will return to this source of error in our discussion of the numerical results in Section 4.2.*

Returning to the issue of the rotations, there are really only two possibilities: either one tries to maximize the likelihood function with respect to  $x$  and  $s$ , or one maximizes the likelihood with respect to  $x$ , averaged over all possible rotations. The approach taken in [34] is the latter, namely one considers

$$f(y_j; \phi(\cdot; x)) := \int_{SO(3)} f(y_j; \phi^s(\cdot; x)) d\mu(s). \quad (45c)$$

Here we use the mean weighted by  $\mu(s)$  to allow for the possibility of weighting the rotations. In the absence of any knowledge about the scattering probability  $\phi^s(\cdot; x)$  one would choose a uniform distribution for the rotations. But if one had a solution  $x^*$  to (39), this could be folded back into (45c) to compute the average over the likelihood of the rotations conditioned on  $x^*$ , effectively assigning a probability distribution to the rotations for each outcome  $y_j$ . Our demonstrations use only a uniform distribution of directions on  $SO(3)$ .

An elementary calculation yields

$$\begin{aligned} \nabla f(y_j; \phi(\cdot; x)) &= \left( \int_{SO(3)} \frac{\partial}{\partial x_i} f(y_j; \phi^s(\cdot; x)) ds \right)_{i=1, \dots, n} \\ &= \left( \int_{SO(3)} f(y_j; \phi^s(\cdot; x)) \sum_{k \in \text{supp}(y_j)} \left( \frac{y_j(k)}{\phi^s(k; x)} - 1 \right) \frac{\partial}{\partial x_i} \phi^s(k; x) ds \right)_{i=1, \dots, n}. \end{aligned} \quad (46a)$$

Another elementary formal manipulation shows that

$$\frac{\partial}{\partial x_i} \phi^s(k; x) := 2\text{Re} \left[ \overline{[\mathcal{F}(\rho(\cdot; x) \circ R(s))]}(k) \cdot \frac{\partial}{\partial x_i} (\mathcal{F}(\rho(\cdot; x) \circ R(s)))(k) \right], \quad k \in \mathbb{R}^2, x \in \mathbb{R}^n. \quad (46b)$$

One last application of the chain rule yields

$$\frac{\partial}{\partial x_i} (\mathcal{F}(\rho(\cdot; x) \circ R(s))) (k) = \left( R(S)^* \mathcal{F}^* \frac{\partial}{\partial x_i} \rho(\cdot; x) \right) (k) \quad k \in \mathbb{R}^2, x \in \mathbb{R}^n. \quad (46c)$$

The parameterization of the electron density  $\rho$  is specified in the next section.

We can now summarize the expression for the gradients of the smooth functions  $g_j(x) := -\log(f(y_j; \phi(x)))$ :

$$\nabla g_j(x) = \frac{-1}{f(y_j; \phi(x))} \nabla f(y_j; \phi(x)) \quad (47)$$

where  $\nabla f(y_j; \phi(x))$  is given by (46a) for  $\frac{\partial}{\partial x_i} \phi^s(k; x)$  given by (46b) and  $\frac{\partial}{\partial x_i} (\mathcal{F}(\rho(\cdot; x) \circ R(s))) (k)$  given by (46c). The resolvent of the subgradient of the constraint-written-as-indicator function  $g_0$  is just the projector onto the set  $C_0$ :

$$J_{g_0,1}(x) := P_{C_0}(x). \quad (48)$$

This is all that is needed to implement Algorithm 1 with  $T_i$  defined by (30).

**Remark 4** (convergence of Algorithm 1 for X-FEL imaging). *Assumptions (a) and (b) of Proposition 1 are easily seen to be satisfied for this application. Indeed, any twice continuously differentiable function satisfies conditions (24) of Example 1. Moreover, if the constraint  $C_0$  is convex, then condition (29) is satisfied with  $\tau_0 = 0$ . Hence the mappings  $T_i$  defined by (30) for the application of X-FEL imaging using model (39) with a smooth parameterization of the electron density  $\rho$  are  $\alpha$ -fne with violation  $\epsilon_i$  and constant  $\alpha_i$  given by (31) for the steps  $t_j$  with  $j > 0$  satisfying (26b). If conditions (a) and (c) of Proposition 1 hold, then we are assured that Algorithm (1) is locally convergent in distribution; if the gauge of metric subregularity is linear, then by Corollary 2 we can expect local linear convergence in the Wasserstein metric. The numerical experiments in Section 4.2 support this conclusion.*

Characterization of the invariant distributions is a topic of future research, but intuitively it should be clear that the more observations  $\{y_1, \dots, y_M\}$  and constraints that can be brought into the objective function (39), the better chance that the set of fixed points of Algorithm 1 will contain only meaningful critical points of (39). The reasoning is as follows: if there is no data, then any feasible parameters  $x \in C_0$  will solve (39). As the number of observations grows, so too grow the number of functions  $g_j$  in the log-likelihood objective, and hence the set of critical points can only shrink. If the set of critical points of (39) consists only of globally optimal solutions, the invariant measures of the randomized algorithm (1) *should* be supported on these solutions. It is an open question to determine exactly when and in what way this holds.

## 4.2 A Numerical Study

A level surface of the electron density used to generate the data for our numerical experiment is shown in Figure 1(a).

The parameterized model for this is simply 10 Gaussian balls where the parameters  $x$  are the centers of the balls:

$$\rho(z; x) := \sum_{i=1}^{10} \mathcal{B}(z; x_i), \quad \text{for} \quad \mathcal{B}(z; x_i) := \sigma * \exp\left(-\frac{1}{2}\|z - x_i\|^2\right) \quad (49)$$

where  $x = (x_1, x_2, \dots, x_{10})$  with each  $x_i = (x_{i1}, x_{i2}, x_{i3}) \in \mathbb{R}^3$  and  $\sigma = 0.519$ . Since the density has the form of Gaussians, the rotated field in the Fourier domain has the explicit formulation [18]

$$(\mathcal{F}(\rho(\cdot; x) \circ R(s))) (k) = \sum_{i=1}^{10} \widehat{\mathcal{B}}(k; (R(s)x)_i) \quad (50a)$$

$$\widehat{\mathcal{B}}(k; (R(s)x)_i) = \sqrt{2\pi}\sigma \exp(-2\pi^2\|k\|^2) \exp(-2\pi i k \cdot (R(s)x_i)) \quad (50b)$$

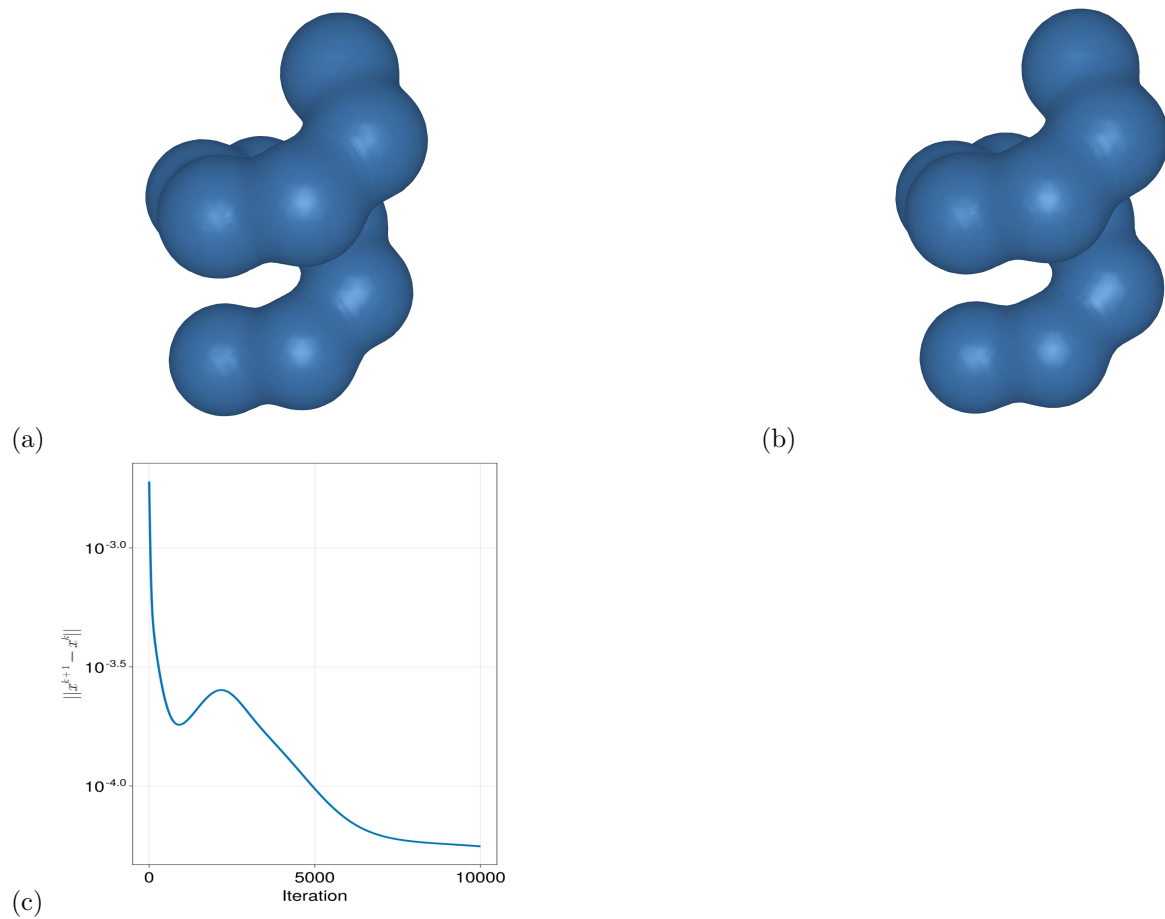


Figure 1: Deterministic recovery. Algorithm 1 with  $m = M = 10,000$ ,  $t = 0.1$ . (a) The true electron density. (b) The computed electron density at the last iterate using (a) as the starting point. (c) The iterate differences.

where  $i := \sqrt{-1}$ . Just as a reminder,  $k \in \mathbb{R}^3$  is a point in the Fourier domain restricted to a two-dimensional surface  $\mathcal{E}$  which for simplicity we take to be a plane through the origin with a fixed orientation. The gradient (46c) then has the explicit representation

$$\begin{aligned} \frac{\partial}{\partial x_{ir}} (\mathcal{F}(\rho(\cdot; x) \circ R(s))) (k) &= \frac{\partial}{\partial x_{ir}} \sum_{i'=1}^{10} \widehat{\mathcal{B}}(k; (R(s)x)_{i'}) \\ &= -2\pi i \sigma (R(s)k)_r \widehat{\mathcal{B}}(k; R(s)x_{ir}) \quad (r = 1, 2, 3). \end{aligned} \quad (51)$$

For this demonstration we do not introduce any constraints, so here  $C_0 = \mathbb{R}^n$ , and the forward-backward operator (30) reduces to just gradient descent (27).

The numerical experiments were produced in the Julia programming language on 13th generation Intel<sup>TM</sup> CORE<sup>®</sup>i9 CPUs together with Nvidia GPUs. Scripts for generating the numerical experiments are available at [20].

We generated  $M = 10,000$  images/outcomes  $y_j$  so that, on average, each image contained 15 single scattering events across the measurement plane  $\mathcal{E}$ . Figure 1(b)-(c) shows the result of applying Algorithm 1 to the deterministic case:  $m = M = 10,000$  so that the index set  $\mathbb{I} = \{1, 2, \dots, M\}$ , the random variable  $\xi_k$  takes only one value, and the Markov operator reduces to the deterministic fixed point mapping  $T := \frac{1}{M} \sum_{j=1}^M \text{Id} - t \nabla g_j$  where  $\nabla g_j$  is given by (47), (46a), (46b) and (51). The mapping  $T$  has fixed points at the critical points of the objective in (39) and these exist (assumption (a) of Proposition 1) by level-boundedness of the objective. The invariant measures are supported exactly on these critical points:  $\text{supp}(\pi) \subset \text{Fix } T$  for any  $\pi \in \text{inv } \mathcal{P}$ . Assumption (b) of Proposition 1 was shown to hold for all step sizes  $t_j$  small enough by the discussion in Remark 4. The Markov transport discrepancy  $\Psi$  defined by (15) reduces to (35). Convergence in distribution is actually pointwise deterministic convergence, so from any initialization at a single point,  $\mu_0 = \delta_{x^0}$ , condition (17) in Proposition 1 reduces to (38) which, in this case, is the usual deterministic error bound:

$$d(x, \text{Fix } T) \leq \mathcal{G}(\|x - Tx\|) \quad \forall x \in G. \quad (52)$$

Under the assumption that this error bound holds for some gauge  $\mathcal{G}$ , we expect, by Proposition 1 local convergence to a critical point of (39) for all fixed step lengths  $t$  small enough. The step  $t = 0.1$  for these numerical experiments was found by trial-and-error.

The recovered image in Figure 1(b) was obtained from the initialization of the true electron density shown in Figure 1(a). While it is difficult to see from the recovered object, the iterate steps shown in Figure 1(c) indicate that the numerical solution differs from the true object used to construct the model data. There are several possibilities for this discrepancy which will require further study. One obvious source for this difference is that the information about the true object is obtained only through finitely many random samples, so problem (39) is itself a random instance, hence the recovered object, while obtained through a deterministic algorithm, is itself a random variable. The theory presented here can be applied to the limiting case of uncountably infinite collections, i.e. in the limit as the sum in (39) or  $(\mathcal{P})$  converges to an integral. In fact, Assumption 1 and Proposition 1 are based on [16, Assumption 2.1 and Theorem 2.6] which are formulated over possibly uncountably infinite index sets. Convergence of the laws of the iterates of Algorithm 1 for fixed sample sizes  $m$  follows by [16, Theorem 2.6]. The question as to whether the invariant distribution of the Markov operator in this case corresponds to the true distribution  $\rho_*$  has not been addressed here, but we think that this should be true. We will have more to say about this in the concluding remarks. Another possible source of error is the operation of averaging over all possible rotations in (45c). We do not compute the integral in (45c), but rather a discretized sum which introduces some unavoidable error. An even more banal, but not uncommon source of error in practice is an incorrect value for one of the many physical parameters used to construct the mapping  $\mathcal{F}$ . We are confident that with this synthetic example, all such trivial model errors have been eliminated.

Some or all of these sources of error could be at play in practice with real data, but for the present demonstration, these are beside the point. We are focused only on finding solutions to model (39) regardless of the appropriateness of the chosen parameters, so long as bad parameter choices do not change the

mathematical properties of the objective (in particular smoothness). In this context, Figure 1(c) showing the differences between successive iterates on a log-scale indicates local linear convergence to a critical point. In the deterministic setting [24, Theorem 2] has established that metric subregularity of  $\text{Id} - T$  for 0 at fixed points (that is, (52) in an appropriate form) is in fact *necessary* for local linear convergence. Figure 1(c) does not contradict the hypothesis that, in the deterministic case, the transport discrepancy is metrically subregular with a linear rate, in which case the observed local linear convergence in Figure 1(c) is guaranteed by Corollary 2. If the fixed point is, up to rotations, unique, then we can use the iterate differences to obtain an estimate of the distance to the limit at termination. Round-off error for these calculations starts to appear at about  $10^{-5}$  since we are working on single-precision GPU's. This deterministic calculation (10,000 iterations) took several minutes (less than 5).

For the randomized algorithm we sample, respectively, 100, 500, 1000, and 5000 of the total 10,000 images ( $m = 100, 500, 1000$  and  $5000$ ) *without* replacement and run 10 iterations of gradient descent on each batch ( $q = 10$  in (27)). The recovered density  $\rho$  at the last (outer) iteration is shown in Figure 3. Each

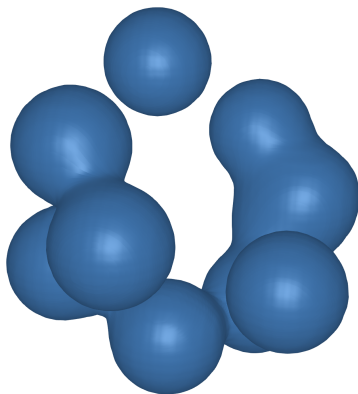


Figure 2: Random initialization.

numerical experiment was initialized by a randomly generated density, an example of which is shown in Figure 2, and ran the same number of inner and outer iterations, namely  $1000 \times 10$ ; this was chosen to match the 10,000 iterations for the deterministic example shown in Figure 1. The compute times for these runs were: 88 seconds for  $m = 100$ , 107 seconds for  $m = 500$ , 139 seconds for  $m = 1000$ , and 418 seconds for  $m = 5000$ . In comparison, the deterministic example with 10,000 iterations and no sampling required 494 seconds.

As Figure 3 demonstrates, the reconstructions at iteration 5000 are very similar, up to rotations and chirality, to the deterministic reconstruction in Figure 1 at iteration 10,000. The Cesàro sum of the iterates and the variance of the iterate shown in Figure 4 was chosen to indicate convergence of the first two moments of the laws of the iterates as predicted in Proposition 1 (or in the linear case 2) since those results provide guarantees for convergence with respect to the Wasserstein-2 probability measure, which yields rates of convergence for the first two moments of the distribution.



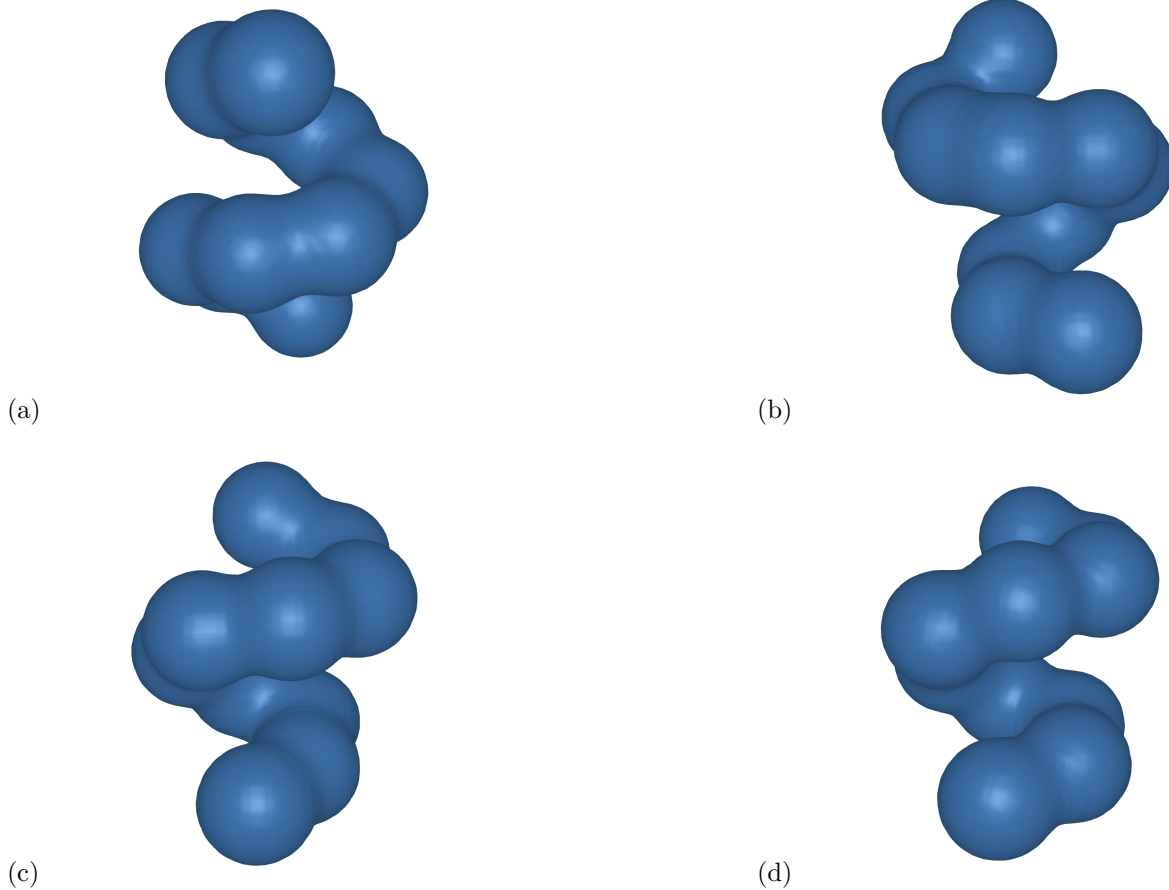


Figure 3: Random recovery. Algorithm 1 with  $T_i$  given by (27) for  $q = 10$  and  $t_j = 0.1$  for all  $j$ . The  $M = 10,000$  images are sampled with  $|I_i| = m$  for (a)  $m = 100$ , (b)  $m = 500$ , (c)  $m = 1000$ , and (d)  $m = 5000$ . Shown are the computed average electron densities at iteration  $k = 5000$ . The compute times for the first 1000 iterations (1000 outer iterations with 10 inner iterations for each outer iteration) runs were: 88 seconds for  $m = 100$ , 107 seconds for  $m = 500$ , 139 seconds for  $m = 1000$ , and 418 seconds for  $m = 5000$ . In comparison, the deterministic example with 10,000 iterations and no sampling required 494 seconds

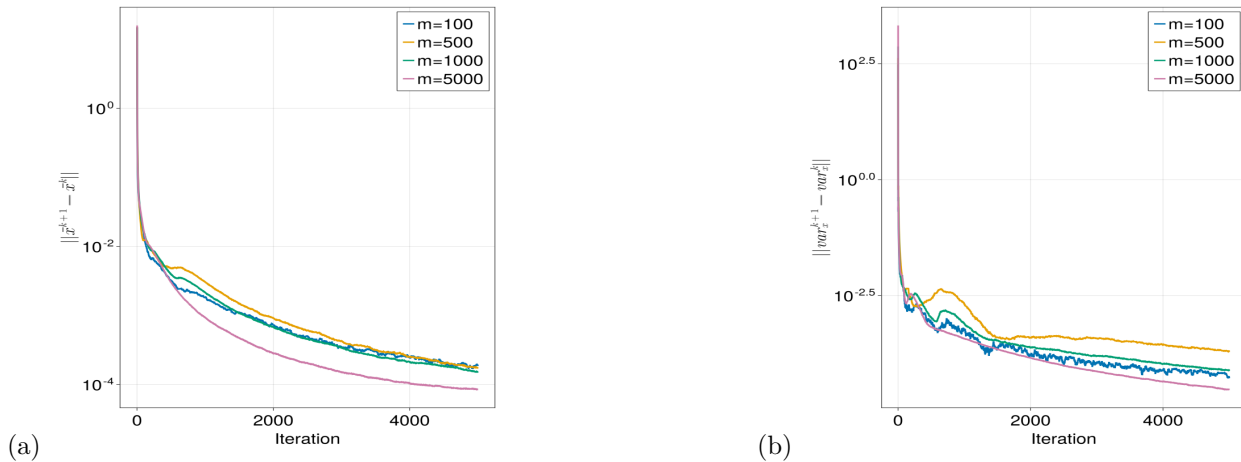


Figure 4: Convergence behavior of the mean (a) and variance (b) of the iterates. Algorithm 1 with  $T_i$  given by (27) for  $q = 10$  and  $t_j = 0.1$  for all  $j$ . The  $M = 10,000$  images are sampled with  $|I_i| = m$  for  $m = 100, 500, 1000$ , and  $5000$ .

## 5 Concluding remarks and open questions

Several issues and directions for future research were mentioned above. To conclude, we summarize these and add to this list. In the context of X-FEL imaging, the directions for further study include: improving the numerical model without increasing the computational complexity (too much); exploring more realistic parameterizations of the electron density; including constraints into the model (39); and testing this approach on experimental data. Regarding 45c, it was mentioned that a solution  $x^*$  can be used to assign a probability distribution to the rotations of each outcome  $y_j$ , which can then be used for the weighted integral in (45c). This is appealing both from the perspective of the application as well as posing interesting mathematical challenges for the analysis of such an approach.

On the mathematical side, there are several difficult issues to tackle. First and foremost is either to develop efficient methods for computing the Wasserstein metric in the convergence statement of Proposition 1, or to develop efficient approximations that can be used to monitor algorithm performance. Second but just as important is to characterize the supports of the invariant measures of the Markov operator behind Algorithm 1 in terms of the critical points of the deterministic problem 39 or, more generally ( $\mathcal{P}$ ). This also has bearing on the analysis of the solutions to (39) in a stochastic context, in other words, in the limit as the sum converges to an integral: are the invariant measures of the Markov operator unique up to rotation and do these correspond to the true probability distribution  $\rho_*$ ? The dependence of the rates of convergence predicted in Proposition 1 on the sample size  $m$  is also an important related issue. Third, and more attainable in the near term is to verify the metric subregularity assumption of the Markov transport discrepancy (17) by verifiable properties of its deterministic counterpart.

## References

- [1] J. B. Baillon, R. E. Bruck, and S. Reich. On the asymptotic behavior of nonexpansive mappings and semigroups in Banach spaces. *Houston J. Math.*, 4(1):1–9, 1978.
- [2] S. Basu and Y. Bresler. Feasibility of tomography with unknown view angles. *IEEE Trans. Image Proc.*, 9(6):1107–1122, 2000.
- [3] S. Basu and Y. Bresler. Uniqueness of tomography with unknown view angles. *IEEE Trans. Image Proc.*, 9(6):1094–1106, 2000.

- [4] P. Billingsley. *Convergence of probability measures. 2nd ed.* Chichester: Wiley, 2nd ed. edition, 1999.
- [5] M. Born and E. Wolf. *Principles of Optics.* Pergamon Press, New York, 6th edition, 1980.
- [6] S. Boutet, L. Lomb, G. J. Williams, T. R. M. Barends, and et al. High-resolution protein structure determination by serial femtosecond crystallography. *Science*, 337(6092):362–4, 7 2012.
- [7] R. E. Bruck and S. Reich. Nonexpansive projections and resolvents of accretive operators in Banach spaces. *Houston J. Math.*, 3(4):459–470, 1977.
- [8] D. Butnariu. The expected-projection method: Its behavior and applications to linear operator equations and convex optimization. *J. Appl. Anal.*, 1(1):93–108, 1995.
- [9] D. Butnariu and S. D. Flăm. Strong convergence of expected-projection methods in Hilbert spaces. *Numer. Funct. Anal. and Optim.*, 16(5&6):601–636, 1995.
- [10] H. N. Chapman, P. Fromme, A. Barty, T. A. White, and et al. Femtosecond X-ray protein nanocrystallography. *Nature*, 470(7332):73–77, 2 2011.
- [11] M. Edelstein. A remark on a theorem of M. A. Krasnoselski. *Amer. Math. Monthly*, 73(5):509–510, May 1966.
- [12] M. Hairer. Ergodic properties of markov processes. *Lecture notes, University of Warwick*, page 47, 2006.
- [13] M. Hairer. Convergence of Markov processes. *Lecture notes, University of Warwick*, page 39, 2021.
- [14] N. Hermer, D. R. Luke, and A. Sturm. Random function iterations for consistent stochastic feasibility. *Numer. Funct. Anal. Optim.*, 40(4):386–420, 2019.
- [15] N. Hermer, D. R. Luke, and A. Sturm. Nonexpansive Markov operators and random function iterations for stochastic fixed point problems. *J. Conv. Anal.*, 30(4):1073–1114, 2023.
- [16] N. Hermer, D. R. Luke, and A. Sturm. Rates of convergence for chains of expansive Markov operators. *Trans. Math. Appl.*, 7(1):tnad001, 12 2023.
- [17] A. D. Ioffe. Nonlinear regularity models. *Math. Program.*, 139(1-2):223–242, 2013.
- [18] A. Jain. *Fundamentals of Digital Image Processing.* Prentice Hall, Englewood Cliffs, NJ, 1989.
- [19] M. A. Krasnoselski. Two remarks on the method of successive approximations. *Math. Nauk. (N.S.)*, 63(1):123–127, 1955. (Russian).
- [20] D. R. Luke. Proxtoolbox. <http://num.math.uni-goettingen.de/proxtoolbox/>, 2017.
- [21] D. R. Luke. Convergence in distribution of randomized algorithms: The case of partially separable optimization. 2023.
- [22] D. R. Luke, S. Sabach, and M. Teboulle. Optimization on spheres: Models and proximal algorithms with computational performance comparisons. *SIAM J. Math. Data Sci.*, 1(3):408–445, 2019.
- [23] D. R. Luke and M. K. Tam. The proximal point algorithm without monotonicity. In *Proceedings of the 35th RAMP Symposium*, pages 39–48, Tokyo, November 2023. Research Association of Mathematical Programming.
- [24] D. R. Luke, M. Teboulle, and N. H. Thao. Necessary conditions for linear convergence of iterated expansive, set-valued mappings. *Math. Program. A*, 180:1–31, 2018.

- [25] D. R. Luke, N. H. Thao, and M. K. Tam. Quantitative convergence analysis of iterated expansive, set-valued mappings. *Math. Oper. Res.*, 43(4):1143–1176, 2018.
- [26] W. R. Mann. Mean value methods in iterations. *Proc. Amer. Math. Soc.*, 4:506–510, 1953.
- [27] J. J. Moreau. Proximité et dualité dans un espace Hilbertien. *Bull. de la Soc. Math. de France*, 93(3):273–299, 1965.
- [28] J. M. Ortega and W. C. Rheinboldt. *Iterative Solution of Nonlinear Equations in Several Variables*. Academic Press, New York, 1970.
- [29] V. M. Panaretos. On random tomography with unobservable projection angles. *Annals of Statistics*, 37(6A):3272–3306, 2009.
- [30] R. A. Poliquin and R. T. Rockafellar. Prox-regular functions in variational analysis. *Trans. Amer. Math. Soc.*, 348:1805–1838, 1996.
- [31] R. A. Poliquin, R. T. Rockafellar, and L. Thibault. Local differentiability of distance functions. *Trans. Amer. Math. Soc.*, 352(11):5231–5249, 2000.
- [32] A.-L. Robisch and T. Salditt. Coherent X-Ray Imaging. In T. Salditt, A. Egner, and D. R. Luke, editors, *Nanoscale Photonic Imaging*, pages 35–70. Springer, Cham, 2020.
- [33] R. T. Rockafellar and R. J. Wets. *Variational Analysis*. Grundlehren Math. Wiss. Springer-Verlag, Berlin, 3 edition, 2009.
- [34] S. Schultze and H. Grubmüller. De novo structural ensemble determination from single-molecule x-ray scattering: A Bayesian approach. 2023.
- [35] A. Singer and H.-T. Wu. Two-dimensional tomography from noisy projections taken at unknown random directions. *SIAM J. Imaging Sci.*, 6(1):136–175, 2013.
- [36] J.E. Spingarn. Submonotone subdifferentials of lipschitz functions. *Trans. Amer. Math. Soc.*, 264:77–89, 1981.
- [37] D.W. Stroock. *Probability Theory: An Analytic View*. Cambridge University Press, 2010.
- [38] T. Szarek. Feller processes on nonlocally compact spaces. *Ann. Probab.*, 34(5):1849–1863, 2006.
- [39] C. Villani. *Optimal transport: Old and New.*, volume 338. Berlin: Springer, 2009.
- [40] B. von Ardenne and H. Grubmüller. Single Particle Imaging with FEL Using Photon Correlations. In T. Salditt, A. Egner, and D. R. Luke, editors, *Nanoscale Photonic Imaging*, pages 435–355. Springer, Cham, 2020.
- [41] B. von Ardenne, M. Mechelke, and H. Grubmüller. Structure determination from single molecule x-ray scattering with three photons per image. *Nature Communications*, 9:2375, 2018.